DOI: 10.1021/ma9013065

Macromolecules
ARTICLE

Nanostructure Formation in Poly(3-hexylthiophene-*block*-3-(2-ethylhexyl)thiophene)s

Yue Zhang,[†] Keisuke Tajima,*[,†] and Kazuhito Hashimoto*[,†,‡]

[†]*Department of Applied Chemistry, School of Engineering, The University of Tokyo, 7-3-1 Hongo, Bunkyo-ku, Tokyo 113-8656, Japan, and* [‡]*HASHIMOTO Light Energy Conversion Project, ERATO, Japan Science and Technology Agency (JST), Tokyo, Japan*

Received June 17, 2009; Revised Manuscript Received August 4, 2009

ABSTRACT: A series of conjugated, highly regioregular poly(3-hexylthiophene-*block*-3-(2-ethylhexyl)-thiophene)s (P(3HT-*b*-3EHT)s) were synthesized by nickel-catalyzed quasi-living polymerization. ^{1}H NMR spectra and GPC charts showed that the synthesized P(3HT-*b*-3EHT)s have well-controlled block ratios and molecular weights with narrow polydispersity indices, which enable the systematic study of the correlation between the polymer structure and nanostructures of P(3HT-*b*-3EHT) films. AFM observation revealed that P(3HT-*b*-3EHT)s self-organized into thin films after thermal annealing to spontaneously form clear microphase-separated nanopatterns whose size depends on the block ratio. The temperature for the nanopattern formation correlated to the transition temperature of the polymers that were investigated by DSC. In contrast, only featureless patterns were observed in the films of random copolymers and physical mixtures of homopolymers with the corresponding unit ratios, indicating that well-defined diblock copolymers are essential for spontaneous nanopattern formation. The UV−vis absorption spectra and XRD patterns obtained showed that highly crystalline P3HT blocks stacked with their π-planes and alkyl side chains aligned in the thin films in an orientation normal to the substrate.

1. Introduction

Controlling the orientation and the nanostructures of semiconducting polymers in solid state is of crucial importance in the development of high-performance polymer electronic devices such as organic field-effect transistors (OFETs)[1,2] and photovoltaic devices (OPVs).[3−7] For example, Sirringhaus et al. reported a strong effect of polymer alignment on hole mobility in OFET films.[8] In OPVs, several groups reported that the thermal annealing of polymer films blended with small molecules induces the formation of a nanoscale interpenetrating network between the components, resulting in a high power conversion efficiency.[9,10] To precisely control this nanostructure in polymer films, one interesting strategy is to use block copolymers (BCPs) containing two different semiconducting polymer blocks. BCPs are well-known to self-organize into 3-D microphase-separated structures[11,12] such as spherical, cylindrical, gyroid or lamellar structures, driven by factors such as immiscibility or the crystallinity difference between the blocks. The control of molecular orientation and the patterning of such microphase separated structures have also been reported.[13] Therefore, BCPs based on highly crystalline, semiconducting blocks with excellent electronic properties such as poly(3-hexylthiophene) (P3HT) can lead to the bottom-up construction of high-performance polymer electronic circuits.

There have been several reports on semiconducting polymer-based BCPs[14−24] combined with polymers such as polystyrene,[15,18] polymethylacrylate,[15] polyethylene,[14] etc. However, the introduction of those insulating blocks dilutes the concentration of the semiconducting blocks in the films, leading to the decline in their electronic conductivity. Sauve et al. reported that the FET mobility of poly(3-hexylthiophene-*b*-methylacrylate) BCPs decreases as polymethylacrylate content increases.[25] In addition, from the synthetic viewpoint, most of the synthetic routes reported so far involve the use of functionalized P3HT as a macroinitiator for the subsequent living radical or anionic polymerization. Hadziioannou et al. reported the nanorod formation of rod−coil diblock copolymers by using poly(phenylenevinylene) derivatives as rod segment macroinitiators, and polystyrene or polybutadiene as a coil-like segment by radical polymerization.[26] Yu et al. reported the fibrous structure formation of diblock oligomers containing both oligo(phenylenevinylene)s and oligothiophenes as rodlike segments.[27] These multistep polymerizations by macroinitiators, however, often suffer from a low efficiency of the initiation reaction that requires the fractionation of the polymers to obtain pure BCPs, and from a large polydispersity index (PDI) that possibly limits the formation of fine nanostructures.

Recently, we reported the synthesis of conjugated, highly regioregular poly[(3-hexylthiophene)-*block*-(3-(2-ethylhexyl)thiophene)]s (P(3HT-*b*-3EHT)s) via modified Grignard metathesis (GRIM) polymerization and observed their microphase separated structures.[28] The GRIM polymerization of 3-alkylthiophenes is a quasi-living chain-growth synthesis recently developed by McCullough et al.[29−31] and further modified by Yokozawa et al.[32] The well-controlled nature of the polymerization enables molecular weight control by changing the amount of Ni catalyst while keeping the PDIs of the polymers narrow. The one-pot synthesis of BCPs with various block ratios is also possible by changing the feed ratio of each monomer. Such narrow PDIs of BCPs will lead to the formation of clear microphase-separated patterns in the films. P(3HT-*b*-3EHT)s are the first reported compounds in which all-conjugated P3HT-based BCPs were used to control the nanostructure. Shortly after our report, Ueda et al. also independently reported a well-controlled rod−rod diblock copolymer poly[(3-hexylthiophene)-*block*-(3-phenoxymethylthiophene)] with a narrow PDI synthesized via a similar route.[33] Ouhib et al. synthesized the block copolymers poly[(3-hexylthiphene)-*block*-(3-tolylthiophene)]s via GRIM polymerization and used them in organic solar cells,[34] although the

*Corresponding authors. E-mail: (K.T.) k-tajima@light.t.u-tokyo.ac.jp; (K.H.) hashimoto@light.t.u-tokyo.ac.jp.

 Published on Web 08/13/2009

detailed synthetic conditions, the polymer characterizations and the observation on the microphase separation were not included in their report.

Here, we systematically studied the relationship between P(3HT-*b*-3EHT) block ratio and nanostructure formation. BCPs with several different molar ratios of the P3HT fraction to the P3EHT fraction were synthesized and characterized to study the usefulness of GRIM polymerization. The evolution of nanopatterns in P(3HT-*b*-3EHT) films was investigated in detail in relation to the thermal behavior of the polymers. In addition, we compared the properties of P(3HT-*b*-3EHT)s with those of the corresponding random copolymers and physical mixtures of the homopolymers to verify the concept of BCP as an essential condition for spontaneous nanopattern formation in the films. AFM observation and X-ray diffraction (XRD) measurement were performed on the films to elucidate the structures and orientation of the polymer chains in nanopatterns. The difference between the crystalline natures of P3HT and P3EHT blocks in P(3HT-*b*-3EHT)s is shown to be an important factor in the thermal induction of microphase separated structures.

2. Results

2.1. Synthesis of Poly(3-hexylthiophene-*block*-3-(2-ethylhexyl)thiophene) Block Copolymers (P(3HT-*b*-3EHT)s) via GRIM Polymerization. The synthetic route for the P(3HT-*b*-3EHT)s is shown in Scheme 1. The GRIM product of 2-bromo-5-iodo-3-hexylthiophene was polymerized with the Ni catalyst to obtain the P3HT living polymer in the first step. Then, the GRIM product of 2-bromo-5-iodo-3-(2-ethylhexyl)thiophene was added to the reaction solution to obtain P(3HT-*b*-3EHT). Although the living nature of GRIM polymerization has been reported,[10] the synthesis of well-defined BCPs has not yet been achieved since it requires careful optimization of reaction conditions such as reaction time and temperature, otherwise deactivation processes could occur in the polymerization. For example, when we conducted the first step in the polymerization at 0 °C or room temperature, dark-purple P3HT precipitates appeared in the reaction mixture. GPC profiles (Figure S1) showed that a

Scheme 1. Synthetic Route for Poly[(3-hexylthiophene)-*block*-(3-(2-ethylhexyl)thiophene)] Block Copolymers ((P3HT-*b*-P3EHT)s)[a]

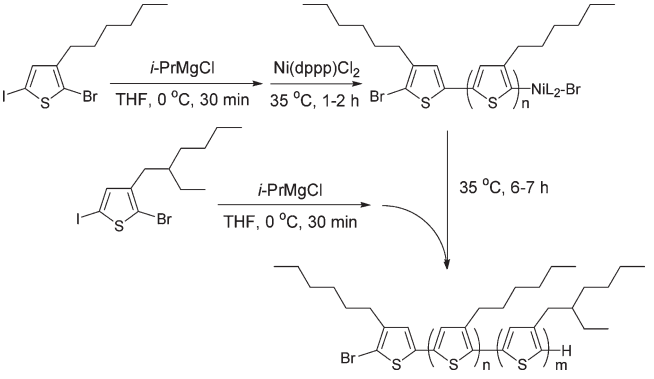

[a] Feed molar ratios of 3-hexylthiophene to 3-(2-ethylhexyl)thiophene are 25:75, 50:50, and 75:25.

fraction of the P3HT prepolymers remains unreacted in the solution after the addition of the second monomer. This is probably due to the termination of the polymerization by the deactivated P3HT precipitates. When we conducted the polymerization at 50 °C, no precipitation was observed; however, GPC profiles indicated the appearance of high-molecular-weight fractions that are probably due to the dimerization of the active sites of P3HT prepolymers or BCPs (Figure S2).

Under the optimized reaction conditions, the first polymerization step was conducted at 35 °C and the second monomer was added immediately after the consumption of the first monomer (Figure S3). As shown in the GPC profiles (Figure S4), all the living P3HTs grew longer with the addition of the second batch of P3HT monomer to give well-defined polymers while keeping their unimodal shape. We adopted the said reaction conditions for the synthesis of P(3HT-*b*-3EHT)s in the following sections.

Three kinds of P(3HT-*b*-3EHT)s with feed molar ratios of 25:75, 50:50, and 75:25 were synthesized. As reference samples, random copolymers P(3HT-*co*-3EHT) with feed molar ratios of 25:75, 50:50, and 75:25 were also synthesized following the route shown in Scheme 2 (see Experimental Section for details). P3HT and P3EHT homopolymers were also synthesized using a similar route. In all polymerizations, the amount of Ni catalyst relative to the total monomer amount was fixed at 1:100 to keep the chain length of the polymers mostly the same.

2.2. Polymer Characterization. *^{1}H NMR spectra and GPC charts.* The composition of the polymers was investigated on the basis of the ^{1}H NMR spectra of P3HT, P3EHT, P(3HT-*b*-3EHT), and P(3HT-*co*-3EHT) as shown in Figure S5. Singlet peaks observed at δ 6.98 and 6.94 ppm were assigned to the sp^2 CH of thiophene rings of 3-hexylthiophene (3HT) and 3-(2-ethylhexyl)thiophene (3EHT) units in the polymers, respectively. Triplet peaks at δ 2.80 ppm and doublet peaks at δ 2.74 ppm were assigned to the sp^3 CH_2 attached to the thiophene rings of 3HT and 3EHT units, respectively. The molar ratios of the 3HT fraction to the 3EHT fraction in P(3HT-*b*-3EHT)s and P(3HT-*co*-3EHT)s were calculated from the integration of the peaks in both regions, which were close to the feed molar ratios of 25:75, 50:50, and 75:25 summarized in Table 1. The regioregularity of each polymer was more than 97%, as confirmed from the peak integration of ^{1}H NMR between 6.98, 6.94, and 7.05 ppm.[35] These results suggest that the reactivity and regioselectivity of 3EHT in polymerization are similar to those of 3HT.

GPC traces of the P3HT living prepolymer and P(3HT-*b*-3EHT) are shown in Figure S6. Note that the reaction mixtures were quenched with 50 wt % aqueous HCl at each stage of polymerization and subjected to the measurements without fractionation. The peaks shift to higher molecular weights while maintaining their unimodal shapes, indicating the production of the P(3HT-*b*-3EHT)s with little P3HT homopolymer contamination in the reaction solutions. The BCPs with block ratios of 20:80, 56:44 and 83:17 all showed similar *M*n values of around 20000 with narrow PDIs of 1.10−1.17 without any fractionation, as summarized in Table 1. These results indicate the successful one-pot synthesis

Scheme 2. Synthetic route of Poly(3-hexylthiophene-*co*-3-(2-ethylhexyl)thiophene)) Random Copolymers (P(3HT-*co*-3EHT)s[a]

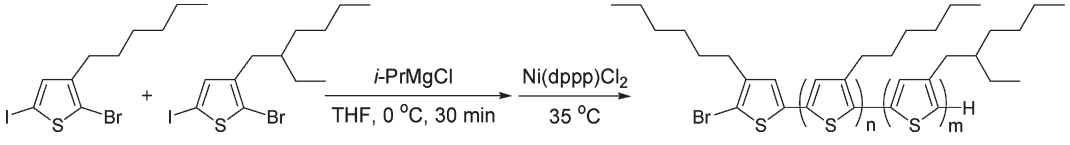

[a] Feed molar ratios of 3-hexylthiophene to 3-(2-ethylhexyl)thiophene are 25:75, 50:50, and 75:25.

Table 1. Summary of ^{1}H NMR and GPC Measurements of P3HT and P3EHT Homopolymers, P(3HT-*b*-3EHT)s (without Fractionation) and P(3HT-*co*-3EHT)s

polymer	3HT:3EHT[a]	3HT:3EHT[b]	M_n	M_w	M_w/M_n (PDI)
P3HT	100:0	100:0	22000	26500	1.20
P3EHT	0:100	0:100	17300	21200	1.23
P(3HT-*b*-3EHT)	25:75	20:80	21600	23800	1.10
	50:50	56:44	20400	22300	1.10
	75:25	83:17	20400	24000	1.17
P(3HT-*co*-3EHT)	25:75	25:75	31700	38100	1.20
	50:50	56:44	30300	36300	1.20
	75:25	75:25	30100	35900	1.20

[a] Feed molar ratio. [b] Measured by ^{1}H NMR.

of regioregular P(3HT-*b*-3EHT)s by quasi-living GRIM polymerization. The molecular weights of the homopolymers and random copolymers are also summarized in Table 1.

2.3. Thermal Properties. The thermal properties of P3HT and P3EHT, P(3HT-*b*-3EHT)s, and P(3HT-*co*-3EHT)s and physical mixtures of the homopolymers (see Experimental Section) were investigated by differential scanning calorimetry (DSC). The results are summarized in Table 2, and the DSC traces are presented in Figures S7 and S8. The P3HT homopolymer showed a melting point (T_m) and a recrystallization temperature (T_r) of 239 and 208 °C with the scanning rate of 10 K min^{-1}, respectively, indicating its crystalline nature, as previously reported.[28] In contrast, the P3EHT homopolymer showed a glass temperature (T_g) of only 110 °C under the same conditions. At a lower scanning rate of 2 K min^{-1}, an exothermic peak in the heating process was observed at 55 °C, which could be attributed to the slow recrystallization of P3EHT homopolymer. The melting of the crystalline phase appeared at 91 °C during the subsequent heating process with H_m of 5.9 J g^{-1}, which is much smaller than that of P3HT homopolymer (19.3 J g^{-1}). These results indicate the lower crystallinity of P3EHT homopolymer, which could be attributed to the poor molecular packing between the thiophene rings due to the branched alkyl side chains in the polymer.

P(3HT-*co*-3EHT)s synthesized by the random copolymerization of two monomers showed a relatively simple thermal behavior, as shown in Table 2. They showed single T_m and T_r at all the ratios of the monomer units. Decreasing the ratio of the 3HT unit simply lowered T_m, T_r, and the heats of melting (H_m) and recrystallization (H_r). This is due to the decline in the crystallinity of the polymer chains with the introduction of the low-crystallinity 3EHT fraction into the random copolymers.

In physical mixtures of P3HT and P3EHT homopolymers, polymers are expected to undergo phase-separation in bulk mixture since their crystallinity is totally different from each other. Therefore, the thermal behaviors of the physical mixtures in Table 2 could be explained by the independent melting and recrystallization of the homopolymers. The sets of T_m and T_r that appeared in the high temperature range of 186−229 °C could be attributed to P3HT, while those in the range of 47−86 °C could be attributed to P3EHT. The changes in H_m and H_r agree with the changes in the ratios of P3HT to P3EHT in the mixtures, which support the independent thermal behaviors due to macro-phase separation.

P(3HT-*b*-3EHT)s showed more complicated thermal behaviors depending on the block ratio, which are totally different from those of P(3HT-*co*-3EHT)s or the physical mixtures. For the BCP with the block ratio of 56:44, two endothermic peaks were observed at 211 and 232 °C during the heating process. An exothermic peak at 177 °C was

Table 2. Summary of DSC Measurements of P3HT and P3EHT Homopolymers, P(3HT-*b*-3EHT)s, P(3HT-*co*-3EHT)s, and Physical Mixtures[a]

Polymer	3HT:3EHT[a]	Tm/°C (Hm/J g^{-1})		Tr/°C (Hr/J g^{-1})	
		T1 (H1)	T2 (H2)	T1 (H1)	T2 (H2)
P3HT	100:0	239 (19.3)	-	208 (16.6)	-
P3EHT	0:100	-[b]	-	-	-
P(3HT-*b*-3EHT)	20:80	-	-	103 (2.1)	-
	56:44	232 (3.2)	211 (6.6)	177 (9.8)	-
	83:17	239 (1.8)	228 (9.6)	197 (16.9)	-
P(3HT-*co*-3EHT)	25:75	99 (12.2)	-	54 (6.5)	-
	56:44	144 (15.4)	-	107 (16.0)	-
	75:25	187 (17.4)	-	158 (19.0)	-
Physical mixture	25:75	225 (3.7)	86 (8.0)	186 (4.6)	47 (7.8)
	50:50	228 (8.3)	79 (3.8)	192 (5.3)	49 (3.6)
	75:25	229 (14.6)	76 (1.2)	195 (13.2)	-

[a] measured by 1H-NMR; [b] only a glass transition was observed at 110 °C; - none or no clear peak [a] T_m: melting point. H_m: heat of melting. T_r: recrystallization temperature. H_r: heat of recrystallization (scan rate: 10 K min^{-1}).

observed during the cooling process, indicating the recrystallization of the BCP. This temperature was significantly lower than that of the P3HT homopolymer (208 °C). P(3HT-*b*-3EHT) with the block ratio of 83:17 also showed two endothermic peaks at 228 and 242 °C and an exothermic peak at 197 °C. For the BCP with the block ratio of 20:80, a recrystallization peak was observed at 103 °C in the cooling process, while no clear melting peak was observed in the heating process.

P(3HT-*b*-3EHT)s with a high P3HT block content showed T_m and T_r close to those of the P3HT homopolymer, indicating the segregation of crystalline P3HT blocks in BCPs. The origin of the first T_m in P(3HT-*b*-3EHT)s is not yet clear; polarized optical microscopy (POM) observation on the BCPs did not show any clear liquid crystal phase transitions, but the preliminary results of the variable temperature X-ray diffraction (VT-XRD) showed the presence of a lamellar structure at the temperatures in between the first and the second T_m. Although further investigations are necessary to elucidate the details of the transition, it could be related to the formation of mesophases in which the melting of the P3EHT block occurs while the P3HT block has a lamellar order.

2.4. Film Characterization. *2.4.1. AFM Images.* Thin films of the regioregular P(3HT-*b*-3EHT)s, P(3HT-*co*-3EHT)s, and the physical mixtures of P3HT and P3EHT were prepared by spin coating from chlorobenzene solutions (see Experimental Section). Film thickness was estimated to be 13 nm by X-ray reflectrometry (XRR). Film roughness and surface morphology were observed by atomic force microscopy (AFM) to study nanopattern formation. All the AFM measurements were conducted at room temperature after the thermally annealed samples were cooled down. The film roughness of all samples was less than 5 nm.

Before thermal annealing, a flat surface with no phase pattern was observed in all the samples (not shown). AFM phase images were observed after thermal annealing at several different temperatures for 5 min. As shown in Figure 1, when annealing temperature was changed from 100 to 230 °C for P(3HT-*b*-3EHT) with the block ratio of 83:17, the sample showed small disordered aggregates with a size of several nanometers. When annealed at 240 °C, AFM showed a clear nanopattern with wormlike structures. This threshold temperature exists in between the first (228 °C) and second (242 °C) endothermic peaks of P(3HT-*b*-3EHT). At 250 °C (above the melting point of the polymer), the films showed a somewhat disordered structure. A similar tendency was also observed in P(3HT-*b*-3EHT) with the block ratio of

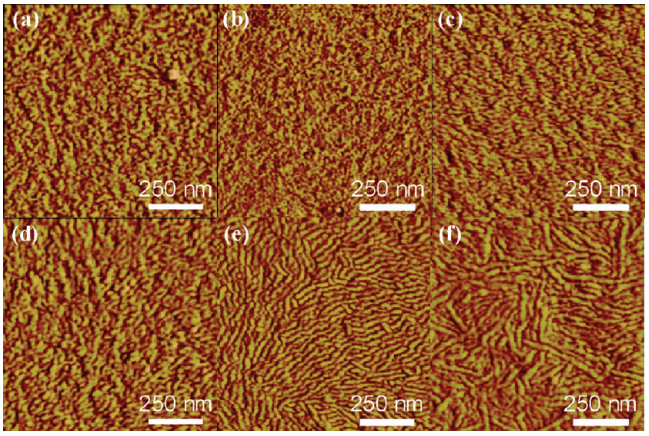

Figure 1. Atomic force microscopy (AFM) phase images of thin solid films of the P(3HT-*b*-3EHT)s with the P3HT molar ratio of 83% during the thermal process. Annealing temperatures are (a) 100, (b) 200, (c) 220, (d) 230, (e) 240, and (f) 250 °C (image size: 1 μm × 1 μm).

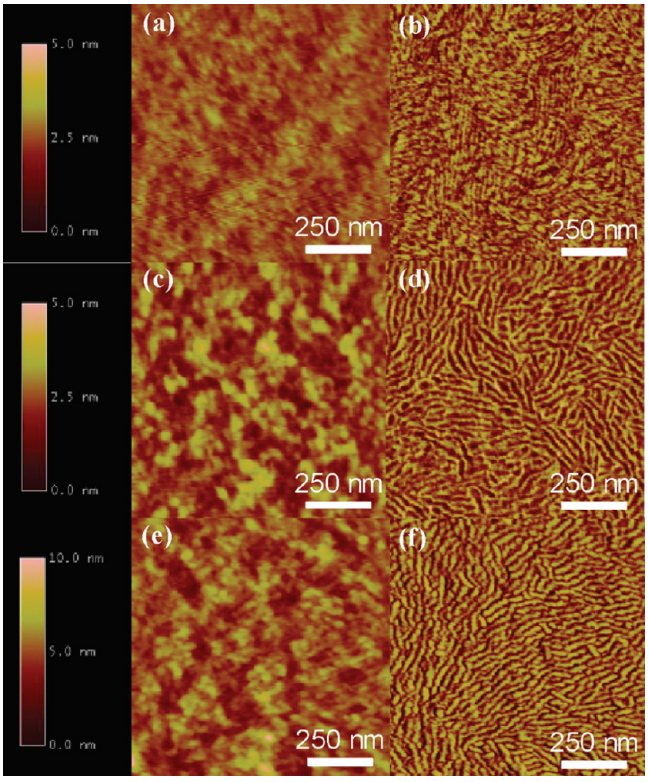

Figure 2. Atomic force microscopy (AFM) height (a, c, and e) and phase (b, d, and f) images of thin films of the P(3HT-*b*-3EHT)s with block ratios of (a and b) 20:80 after annealing at 150 °C, (c and d) 56:44 after annealing at 220 °C and (e and f) 83:17 after annealing at 240 °C (image size: 1 μm × 1 μm).

56:44, which showed the clearest feature at 220 °C, again the temperature between the two endothermic peaks. These results led us to the hypothesis that the melting of a relatively unstrained P3EHT block at high temperatures makes polymer chains more mobile, which can enhance the molecular packing of P3HT blocks to form thermodynamically stable microphase-separated structures.

The phase images of P(3HT-*b*-3EHT)s with all the block ratios showed wormlike structures with widths of several nanometers after annealing at the optimal temperatures (Figures 2b, d, and f), while the height images remained very flat (Figures 2a, c, and e). Considering the large difference in

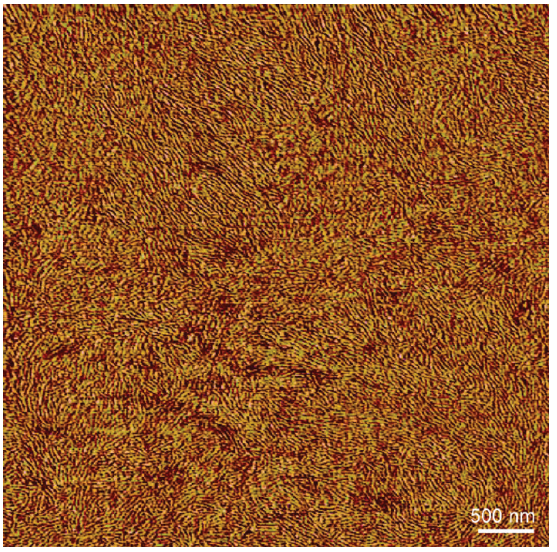

Figure 3. AFM phase image of the thin film of the P(3HT-*b*-3EHT) with the block ratio of 83:17 (image size: 5 μm × 5 μm).

crystallinity between the blocks, these nanostructures can be attributed to the microphase separation of the crystalline (P3HT) and amorphous (P3EHT) blocks. The sizes of the bright and dark domains in the AFM phase images depended on the block ratio of the P3HT content to the P3EHT content of P(3HT-*b*-3EHT)s. P(3HT-*b*-3EHT) with the block ratio of 20:80 showed thin fibers of the bright domains with a width of about 5 nm, while those with the block ratios of 56:44 and 83:17 showed shorter wormlike bright domains with widths of around 10 and 15 nm, respectively. This difference in images also suggests that the bright and dark domains consist of P3HT and P3EHT blocks, respectively.

For P(3HT-*b*-3EHT) with the block ratio of 83:17, a clear microphase-separated nanopattern was observed in the whole area of 5 μm × 5 μm (Figure 3). Moreover, there seems to be some local orientation of wormlike structures. This could provide a possibility to align the nanostructures in one direction, leading to interesting anisotropic physical properties of organic electronic devices.

In contrast, thin films of P(3HT-*co*-3EHT)s with all the component ratios showed dotted patterns with sizes of 30−50 nm after thermal annealing (Figure 4). The patterns were alike even when the molar ratios were changed. AFM images of the physical mixtures of P3HT and P3EHT showed dotted patterns with larger domain sizes of 80−100 nm (Figure 5), probably owing to the macro-phase separation of P3HT and P3EHT. These observations strongly suggest that the covalent attachment of well-defined blocks of P3HT and P3EHT is important in achieving a microphase-separated structure with highly crystalline domains.

2.4.2. UV−Vis Absorption Spectra. Figure 6 showed the UV−vis absorption spectra of the thin films of P(3HT-*b*-3EHT)s. With the block ratio of 20:80, an absorption peak was observed at around 520 nm before thermal annealing (Figure 6a). After the annealing, the absorption peak area slightly decreased, but the spectrum shape did not change. It is known that the films of the regioregular poly(3-alkylthiophene)s often show absorption shoulders in the longer wavelength region (570−610 nm), which has been attributed to the formation of the interchain excited state in the ordered films.[36] The lack of the absorption shoulder in the BCP could be attributed to the large fraction of the less crystalline P3EHT block with weak intermolecular $\pi-\pi$ interaction. With the block ratio of 56:44 (Figure 6b), the

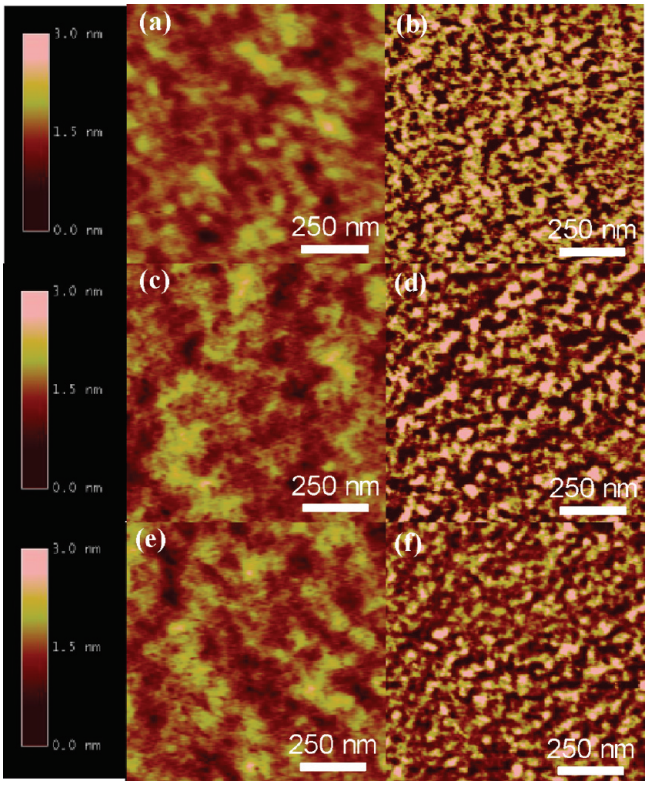

Figure 4. Atomic force microscopy (AFM) height (a, c and e) and phase (b, d and f) images of the thin films of the P(3HT-*co*-3EHT)s with the molar ratios of (a and b) 25:75 after annealing at 110 °C, (c and d) 56:44 after annealing at 150 °C, and (e and f) 75:25 after annealing at 200 °C (image size: 1 μm × 1 μm).

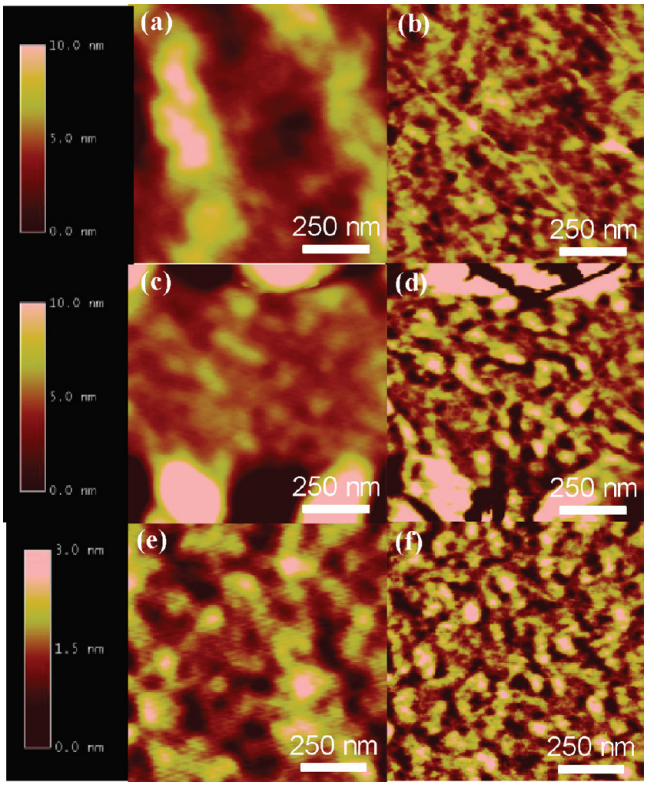

Figure 5. Atomic force microscopy (AFM) height (a, c and e) and phase (b, d, and f) images of the thin films of the physical mixtures of P3HT and P3EHT homopolymers with the molar ratios of (a and b) 25:75, (c and d) 50:50, and (e and f) 75:25 after annealing at 220 °C (image size: 1 μm × 1 μm).

absorption shoulders were observed before the annealing, and their intensities increased after the annealing. The spectral change was most significant at 220 °C, which is between two endothermic peaks at 232 and 211 °C and also gives the most distinct nanostructure patterns in the AFM images as described above. Annealing at 250 °C (above the melting point) greatly decreased the absorption peak area. P(3HT-*b*-3EHT) with the block ratio of 83:17 showed a similar tendency but its spectral change was more pronounced (Figure 6c). Three peaks with peak apexes at 520, 560, and 610 nm were also observed after annealing at 240 °C. The absorption shoulder at around 610 nm could be attributed to the strong intermolecular $\pi-\pi$ interaction and therefore the high crystallinity of the P3HT block.[36] For comparison, we also measured the UV−vis absorption spectra of a thin film of the P3HT homopolymer (Figure S9). Interestingly, the relative intensity of the absorption shoulder was much higher for P(3HT-*b*-3EHT) with the block ratio of 83:17 than for the P3HT homopolymer. This indicates that the P3HT domain in the P(3HT-*b*-3EHT) films had a higher order, although the amount of its crystalline P3HT fraction is reduced to 83% of the total polymer chain. It is suggested that the formation of an ordered self-organization of P3HT segments can be enhanced by the relatively unconstrained P3EHT segments attached to the P3HT homopolymer, resulting in a microphase-separated nanostructure.

The UV−vis absorption spectra of the random copolymers and physical mixtures are shown in Figures S10 and S11. They showed a small absorption shoulder compared with BCPs, which indicates a weak intermolecular $\pi-\pi$ interaction of the polymer chains. The random introduction of 3EHT units in the copolymers or the mixing of the homopolymers could disturb the intermolecular packing of the polythiophene backbones and the alkyl side chains, resulting in the less ordered structures. These results coincide well with the low crystallinity of the random copolymers shown by DSC in the previous section.

2.5. Wide-Angle X-ray Diffraction Measurement. X-ray diffraction (XRD) measurement was performed on the thin film of P(3HT-*b*-3EHT) with the block ratio of 83:17 after annealing at 240 °C, with P3HT and P3EHT homopolymers as references for analyzing the horizontal and vertical molecular packings and orientations of BCP (Figure 7). The P3HT film showed distinct diffraction peaks at 2θ of 5.08, 10.60 and 15.88° in the out-of-plane measurement and in the 23.26° in the in-plane measurement. These peaks can be assigned to a lamellar structure with lattice constants of 1.69 and 0.382 nm for the (*h*00) and (0*h*0) planes, respectively. These values are close to those reported for P3HT thin films.[37,38] This result indicates that alkyl side chains of P3HT are oriented vertical to the substrate to form an edge-on orientation, while the intermolecular $\pi-\pi$ stacking between the thiophene rings is parallel to the glass substrate.

The thin film of the P3EHT homopolymer showed diffraction peaks at 5.96 and 11.92° in the out-of-plane measurement, which correspond to an interlayer distance of 1.48 nm. This is smaller than that of the P3HT homopolymer. A very weak diffraction peak at 17.3° was observed in the in-plane measurement, which could be assigned to a $\pi-\pi$ stacking distance of 0.512 nm. These observations suggest that the twist of the thiophene rings and the inefficient packing of the bulky 2-ethylhexyl side chains result in the shorter interlayer distance and poor packing of thiophene rings in P3EHT films.

The thin film of P(3HT-*b*-3EHT) with the block ratio of 83:17 after annealing showed almost identical XRD patterns to

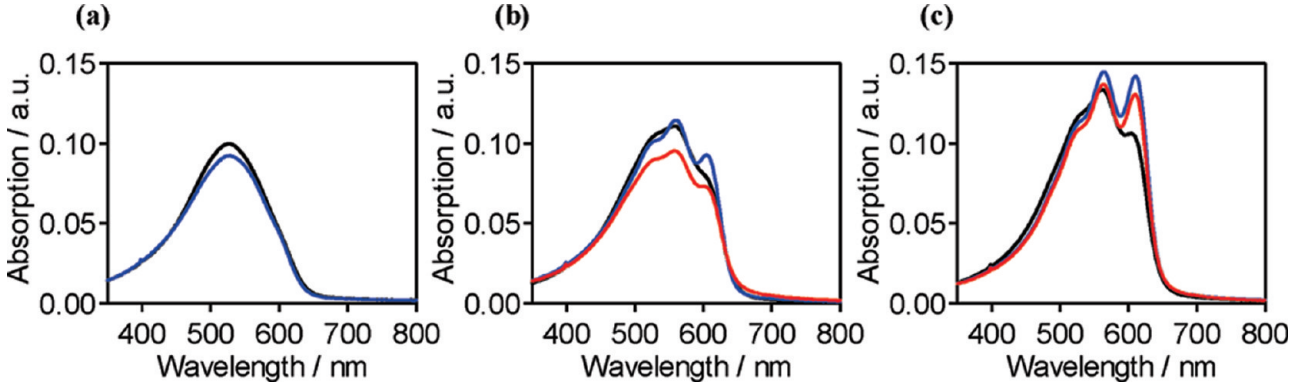

Figure 6. UV−vis spectra of thin solid films of BCPs with the P3HT block ratios of (a) 20% after annealing at 80 °C (black) and 150 °C (blue), (b) 56% before (black) and after annealing at 220 °C (blue) and 250 °C (red), and (c) 83% before (black) and after annealing at 240 °C (blue) and 250 °C (red).

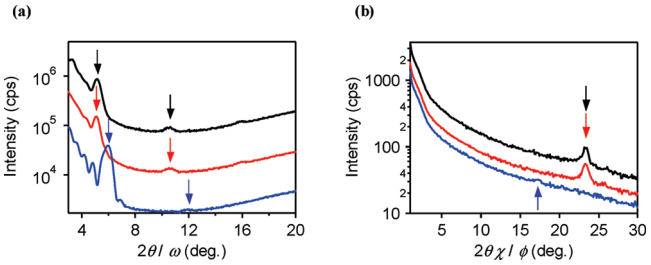

Figure 7. XRD patterns along the (a) out-of-plane and (b) in-plane axes of the thin solid films of P(3HT-*b*-3EHT) with 83% P3HT block ratio (black), P3HT (red) homopolymer, and P3EHT (blue) homopolymer.

the P3HT homopolymer in both the in-plane and out-of-plane measurements. This indicates that P3HT blocks form a layer crystalline structure with strong orientations similarly to P3HT homopolymer. In contrast, the diffraction peaks observed for P3EHT were absent in P(3HT-*b*-3EHT), suggesting the less crystalline structures of P3EHT blocks in P(3HT-*b*-3EHT) than of the homopolymer. This might be explained by the molecular weight difference between the P3EHT blocks in P(3HT-*b*-3EHT) (ca. 17% of M_n = 20400) and the P3EHT homopolymer (M_n = 17300). Considering the film thickness of 13 nm measured by XRR, about seven to eight layers of the polymer chains stacked vertical to the substrate.

3. Discussion

Computational calculations based on the density functional theory (DFT) with periodic boundary condition (PBC) were conducted to predict the molecular conformations of regioregular P3HT and P3EHT in order to further understand the nanostructure formation of BCPs (Figure 8). The optimized structure of the P3HT chain under 1-D PBC shows that thiophene rings form a planar structure with their hexyl side chains extended in the same π-plane, which is consistent with the known planar structure of P3HT in solid state.[37,39,40] This result is also consistent with the previous calculations in which bithiophene or bihexylthiophene forms twisted structure with the torsional defect between the neighboring thiophenes,[41,42] while oligo- or poly(hexylthiophene) tends to form planar structure as a result of the stabilization of the broader π-conjugated system.[41,42] In contrast, the optimized P3EHT conformation showed that neighboring thiophene rings twist each other with a dihedral angle of 25° probably because of the steric hindrance of branched alkyl chains. The twisting between neighboring thiophene rings in the main chain could hinder the ordered molecular packing in the films, as experimentally suggested by the results of UV−vis absorption spectra and DSC measurements. Although these

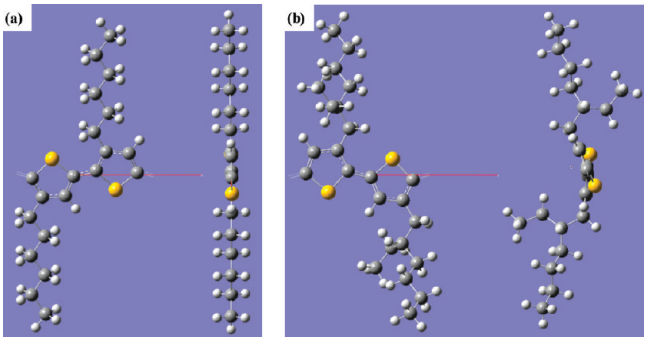

Figure 8. Periodic crystal structures of (a) P3HT and (b) P3EHT polymer blocks predicted by PBC-DFT calculation. Repeat units were viewed vertical to the π-plane (left-hand side in parts a and b) and along the polymer chains (right-hand side in parts a and b). Yellow, gray, light gray balls represent sulfur, carbon and hydrogen atoms, respectively. The red lines along the polymer chain showed the primitive vectors of the repeat units.

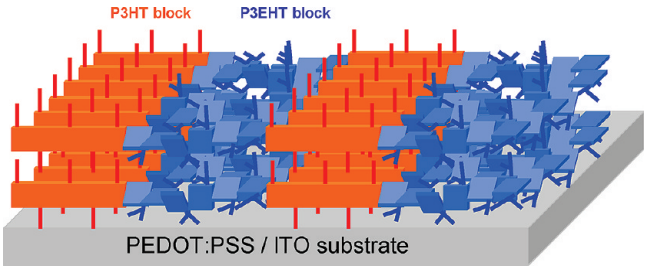

Figure 9. Schematic representation of the proposed film structure of P(3HT-*b*-3EHT) with 83% P3HT block ratio after thermal annealing.

calculation results do not include the intermolecular interactions that are responsible for the solid state, they at least suggest a less ordered nature of P3EHT domains than of P3HT domains in diblock copolymer films.

From the above results including the AFM phase images and XRD profiles, we propose the microphase-separated structure of P(3HT-*b*-3EHT) films as schematically shown in Figure 9. After thermal annealing, the P3HT and P3EHT blocks separated from each other to self-assemble into bright and dark domains in the AFM phase images, respectively. Crystalline P3HT polymer chains showed an ordered molecular packing with their alkyl side chains aligned normal to the substrate in the thin films shown as the orange domain in Figure 9. On the other hand, chemically bonded P3EHT blocks segregated to form less crystalline domains shown as the blue domain in Figure 8. The formation of the

nanopattern in AFM images coincided well with the enhancement of the interchain interaction monitored by UV−vis absorption spectral measurement. The dependence on annealing temperature indicated that nanostructure formation occurred at temperatures between those of the first and second endothermic peaks monitored by DSC measurement. These results suggest the formation of a mesophase by the melting of the P3EHT blocks, enhancing the packing of the P3HT blocks.

All the P(3HT-*b*-3EHT)s synthesized in this study showed similar wormlike patterns after the thermal annealing of the films. Similar nanopatterns were also observed in the semiconducting-insulating BCPs P(3HT-*b*-(*t*-butyl)methacrylate),[24] P(3HT-*b*-isoprene),[18] and P(3HT-*b*-styrene)[18,20] synthesized by McCullough et al. Those patterns were observed in the as-cast films and no effects of the thermal annealing on the phase separation of the films were reported. Stingelin-Stutzmann et al. reported the thermal behavior of crystalline−crystalline diblock copolymers (P(3HT-*b*-ethylene)).[21] Their nanostructures in the films could be controlled by adjusting the temperatures for casting from the solution, strongly depending on which block (P3HT or polyethylene) first crystallized from the solvent during the film formation, but no annealing effects were reported in the films. Very recently, Jenehke et al. reported the synthesis and characterization of poly(3-butylthiophene-*b*-3-octylthiophene)s (P(3BT-*b*-3OT))s in which both blocks have a crystalline nature.[43] Although the XRD measurement of the films of P(3BT-*b*-3OT)s indicated the presence of two separated crystalline domains corresponding to P3BT and P3OT, the annealing temperature for the films was well above the melting point of the polymers (280 °C) and fiber-like images rather than microphase-separated images were reported for the films. Although further investigation is still needed to clarify the necessary conditions for microphase separation in semiconducting BCPs, the observations in the current study suggest that the difference in crystallinity in between the P3HT and P3EHT blocks could be an important factor for achieving clear thermally induced microphase-separated structures with highly crystalline domains.

4. Conclusion

We designed and synthesized all-conjugated P(3HT-*b*-3EHT) diblock copolymers and studied their microphase separation formation. Surface morphological, absorption spectral and X-ray studies showed that the crystalline P3HT blocks showed a highly ordered molecular packing in the BCP thin film. Considering the importance of the crystallinity and orientation of the molecules in charge transport, the results provide a clue to developing a strategy for designing the polymers suitable for high-performance electronic devices by spontaneous nanostructure formation.

5. Experimental Section

All reagents were used as received, unless otherwise stated. 3-Bromothiophene, 1-bromohexane, 1-bromo-2-ethylhexane, anhydrous THF, magnesium turnings, Ni(dppp)Cl_2, iodine, *N*-bromosuccinimide (NBS) and *i*-PrMgCl in THF (2 mol/L) were purchased from Wako Pure Chemical Industries, Ltd. Iodobenzene diacetate was purchased from Kanto Chemical Co., Inc. 3-Hexylthiophene, 2-bromo-3-hexylthiophene, 2-bromo-3-hexyl-4-iodothiophene and poly(3-hexylthiophene) were synthesized as previously reported.[13] 3-(2-Ethylhexyl)thiophene, 2-bromo-3-(2-ethylhexyl)thiophene, 2-bromo-3-(2-ethylhexyl)-5-iodothiophene and poly(3-(2-ethylhexyl)thiophene were synthesized following ref 28.

5.1. Synthesis. *Poly(3-hexylthiophene-block-3-(2-ethylhexyl)-thiophene*). The feed molar ratio of 3-hexylthiophene to 3-(2-ethylhexyl)thiophene was changed from 25:75 to 75:25. The molecular weights were controlled by fixing the ratio of the amount of Ni catalyst to the total monomer amount at 1:100. The typical synthesis procedure of P(3HT-*b*-3EHT) diblock copolymers (feed molar ratio of 50:50) was as follows: two round-bottomed flasks (100 mL) equipped with a three-way stopcock were dried by heating under reduced pressure and cooled to room temperature. 2-Bromo-3-hexyl-5-iodothiophene (0.75 g, 2 mmol) was placed in one of the flasks under N_2 atmosphere, and then evacuated under reduced pressure to remove water and oxygen inside. After adding dry THF (20 mL) into the flask via a syringe, the solution was mixed at 0 °C. Two mol/L solution of *i*-PrMgCl in THF (1 mL, 2 mmol) was added via a syringe, and the mixture was stirred at 0 °C for 30 min (solution A). In another flask, 2 mmol of 3-(2-ethylhexyl)thiophene was reacted with *i*-PrMgCl in the same manner (solution B). Solution A was heated up to 35 °C and Ni(dppp)Cl_2 catalyst (21.69 mg, 0.04 mmol) was added in one portion. After stirring for 1 h, solution B was added to solution A via a syringe, and the resulting solution was stirred for 7 h. The reaction was quenched by pouring aqueous HCl (50 wt %) into the solution. The crude polymer was successively washed by Soxhlet extraction using methanol and hexane, and finally extracted using $CHCl_3$. The solvent was removed by evaporation to give a purple solid (0.52 g, 71%). P(3HT-*b*-3EHT)s with feed molar ratios of 25:75 and 75:25 were also synthesized in the same manner to give a purple solid (0.31 g, 41% for 25:45 and 0.47 g, 67% for 75:25) as the final product.

Poly(3-hexylthiophene-co-3-(2-ethylhexyl)thiophene). The feed molar ratio of 3-hexylthiophene to 3-(2-ethylhexyl)thiophene was changed from 25:75 to 75:25. The molecular weights were controlled by fixing the ratio of the amount of Ni catalyst to the total monomer amount at 1:100. The typical synthesis procedure of P(3HT-*co*-3EHT) random copolymers (feed molar ratio of 50:50) was as follows: two round-bottomed flasks (100 mL) equipped with a three-way stopcock were dried by heating under reduced pressure and cooled to room temperature. 2-Bromo-3-hexyl-5-iodothiophene (0.38 g, 1 mmol) and 3-(2-ethylhexyl)thiophene (0.4 g, 1 mmol) were placed in one of the flasks under N_2 atmosphere, and then evacuated under reduced pressure to remove water and oxygen inside. After adding dry THF (10 mL) into the flask via a syringe, the solution was mixed at 0 °C. A 2 mol/L solution of *i*-PrMgCl in THF (1 mL, 2 mmol) was added via a syringe, and the mixture was stirred at 0 °C for 30 min. Then, the reaction mixture was heated up to 35 °C and Ni(dppp)Cl_2 catalyst (10.84 mg, 0.02 mmol) was added in one portion. After stirring for 2 h, the reaction was quenched by pouring HCl aq. (50 wt %) into the solution. The crude polymer was successively washed by Soxhlet extraction using methanol and hexane, and finally extracted using $CHCl_3$. The solvent was removed by evaporation to give a purple solid (0.18 g, 50%). P(3HT-*co*-3EHT) with feed molar ratios of 25:75 and 75:25 were also synthesized in the same manner to give a purple solid (0.22 g, 62% for 25:75 and 0.37 g, 82% for 75:25) as the final product.

Physical Mixtures of P3HT and P3EHT (***4***) *Homopolymers*. The molar ratio of P3HT to P3EHT homopolymers was changed from 25:75 to 75:25. The typical mixture procedure of the P3HT-P3EHT physical mixture (molar ratio of 50:50) was as follows: P3HT (3.32 mg) and P3EHT (11.65 mg) were solved in chloroform solution. Ultrasonication was used to enhance the solubility of polymers in chloroform solvent. The mixture was evaporated and dried under vacuum at 40 °C overnight to give a physical mixture with a mixed molar ratio of 50:50. Physical mixtures with mixed molar ratios of 25:75 and 75:25 were also prepared in the same manner.

5.2. Measurement. Gel permeation chromatography (GPC) was performed using a Shimadzu Prominence system equipped with a UV detector using chloroform as the eluent at 40 °C. The chloroform solution used was filtered using a PTFE filter (pore size: 1.0 μm) before sample injection. ^{1}H NMR spectra in $CDCl_3$ were measured using a JEOL Alpha FT-NMR spectrometer equipped with an Oxford superconducting magnet system (500 MHz). UV−vis spectra were recorded using a JACSO V-650 spectrometer. Differential scanning calorimetry (DSC)

was performed using Rigaku DSC 8230 under N_2 flow. Tapping-mode atomic force microscopy (AFM) was performed with Nanoscope III (Digital Instruments, Inc.). X-ray diffraction was recorded using a Rigaku SmartLab diffractometer with a 9 KW rotating anode Cu Kα source. Conformation optimizations based on DFT calculation for P3HT and P3EHT were carried out at the B3LYP/6-31G* level using a Gaussian 03 program.[44]

5.3. Film Preparation. Films of P3HT and P3EHT homopolymers, P(3HT-*b*-3EHT) diblock copolymers, P(3HT-*co*-3EHT) random copolymers, and physical mixtures of P3HT and P3EHT homopolymers are prepared on precleaned glass substrates from chlorobenzene solution (5 g L^{-1}) by spin-coating with the spinning rate of 2500 rpm and the duration time of 30 s. The glass substrates were cut into 2.5×2.5 cm^2, washed by detergent, pure water, acetone, isopropyl alcohol and water in succession. For thermal annealing experiments, the films are prepared separately for each annealing temperature. AFM, UV−vis and XRD were performed on the same sample after being cooled down to room temperature.

6. Acknowledgment. We thank Rigaku Corp. for the XRD measurement. Y.Z. thanks the Ministry of Education, Culture, Sports, Science, and Technology of Japan for financial support and Sasakawa Scientific Grand. This work was partly supported by the Global COE Program "Chemistry Innovation through Cooperation of Science and Engineering", MEXT, Japan.

Supporting Information Available: Figures showing ^{1}H NMR, GPC, DSC and UV−vis plots and the synthetic route. This material is available free of charge via the Internet at http://pubs.acs.org.

References and Notes

(1) Muccini, M. *Nat. Mater.* **2006**, *5*, 605–613.
(2) Di, C. A.; Yu, G.; Liu, Y.; Zhu, D. *J. Phys. Chem. B* **2007**, *111*, 14083–14096.
(3) Blom, P. W. M.; Mihailetchi, V. D.; Koster, L. J. A.; Markov, D. E. *Adv. Mater.* **2007**, *19*, 1551–1566.
(4) Gunes, S.; Neugebauer, H.; Sariciftci, N. S. *Chem. Rev.* **2007**, *107*, 1324–1338.
(5) Zhang, C.; Sun, S. S. *J. Polym. Sci., Part A: Polym. Chem.* **2007**, *45*, 41–47.
(6) Shin, W. S.; Kim, S. C.; Lee, S. J.; Jeon, H. S.; Kim, M. K.; Naidu, B. V. K.; Jin, S. H.; Lee, J. K.; Lee, J. W.; Gal, Y. S. *J. Polym. Sci., Part A: Polym. Chem.* **2007**, *45*, 1394–1402.
(7) Zhou, E. J.; Tan, Z. A.; He, Y. J.; Yang, C. H.; Li, Y. F. *J. Polym. Sci., Part A: Polym. Chem.* **2007**, *45*, 629–638.
(8) Stutzmann, N.; Friend, R. H.; Sirringhaus, H. *Science* **2003**, *299*, 1881–1884.
(9) Yang, X. N.; Loos, J.; Veenstra, S. C.; Verhees, W. J. H.; Wienk, M. M.; Kroon, J. M.; Michels, M. A. J.; Janssen, R. A. J. *Nano Lett.* **2005**, *5*, 579–583.
(10) Reyes-Reyes, M.; Kim, K.; Dewald, J.; Lopez-Sandoval, R.; Avadhanula, A.; Curran, S.; Carroll, D. L. *Org. Lett.* **2005**, *7*, 5749–5752.
(11) Hamley, I. W. *Nanotechnology* **2003**, *14*, R39–R54.
(12) Mao, G.; Ober, C. K. *Acta Polym.* **1997**, *48*, 405–422.
(13) Bang, J.; Bae, J.; Lowenhielm, P.; Spiessberger, C.; Given-Beck, S. A.; Russell, T. P.; Hawker, C. J. *Adv. Mater.* **2007**, *19*, 4552–4557.
(14) Radano, C. P.; Scherman, O. A.; Stingelin-Stutzmann, N.; Muller, C.; Breiby, D. W.; Smith, P.; Janssen, R. A. J.; Meijer, E. W. *J. Am. Chem. Soc.* **2005**, *127*, 12502–12503.
(15) Li, B.; Sauve, G.; Iovu, M. C.; Jeffries-El, M.; Zhang, R.; Cooper, J.; Santhanam, S.; Schultz, L.; Revelli, J. C.; Kusne, A. G.; Kowalewski, T.; Snyder, J. L.; Weiss, L. E.; Fedder, G. K.; McCullough, R. D.; Lambeth, D. N. *Nano Lett.* **2006**, *6*, 1598–1602.
(16) Li, B.; Santhanam, S.; Schultz, L.; Jeffries-El, M.; Iovu, M. C.; Sauve, G.; Cooper, J.; Zhang, R.; Revelli, J. C.; Kusne, A. G.; Snyder, J. L.; Kowalewski, T.; Weiss, L. E.; McCullough, R. D.; Fedder, G. K.; Lambeth, D. N. *Sensors Actuators B: Chem.* **2007**, *123*, 651–660.
(17) Dai, C. A.; Yen, W. C.; Lee, Y. H.; Ho, C. C.; Su, W. F. *J. Am. Chem. Soc.* **2007**, *129*, 11036–11038.
(18) Iovu, M. C.; Craley, C. R.; Jeffries-El, M.; Krankowski, A. B.; Zhang, R.; Kowalewski, T.; McCullough, R. D. *Macromolecules* **2007**, *40*, 4733–4735.
(19) Kros, A.; Jesse, W.; Metselaar, G. A.; Cornelissen, J. *Angew. Chem., Int. Ed.* **2005**, *44*, 4349–4352.
(20) Liu, J. S.; Sheina, E.; Kowalewski, T.; McCullough, R. D. *Angew. Chem., Int. Ed.* **2002**, *41*, 329–322.
(21) Muller, C.; Goffri, S.; Breiby, D. W.; Andreasen, J. W.; Chanzy, H. D.; Janssen, R. A. J.; Nielsen, M. M.; Radano, C. P.; Sirringhaus, H.; Smith, P.; Stingelin-Stutzmann, N. *Adv. Funct. Mater.* **2007**, *17*, 2674–2679.
(22) Verbakel, F.; Meskers, S. C. J.; Janssen, R. A. J. *Chem. Mater.* **2006**, *18*, 2707–2712.
(23) Tu, G. L.; Li, H. B.; Forster, M.; Heiderhoff, R.; Balk, L. J.; Sigel, R.; Scherf, U. *Small* **2007**, *3*, 1001–1006.
(24) Iovu, M. C.; Zhang, R.; Cooper, J. R.; Smilgies, D. M.; Javier, A. E.; Sheina, E. E.; Kowalewski, T.; McCullough, R. D. *Macromol. Rapid Commun.* **2007**, *28*, 1816–1824.
(25) Sauve, G.; McCullough, R. D. *Adv. Mater.* **2007**, *19*, 1822–1825.
(26) de Boer, B.; Stalmach, U.; van Hutten, P. F.; Melzer, C.; Krasnikov, V. V.; Hadziioannou, G. *Polymer* **2001**, *42*, 9097–9109.
(27) Wang, H. B.; Wang, H. H.; Urban, V. S.; Littrell, K. C.; Thiyagarajan, P.; Yu, L. P. *J. Am. Chem. Soc.* **2000**, *122*, 6855–6861.
(28) Zhang, Y.; Tajima, K.; Hirota, K.; Hashimoto, K. *J. Am. Chem. Soc.* **2008**, *130*, 7812–7813.
(29) McCullough, R. D. *Adv. Mater.* **1998**, *10*, 93–116.
(30) Loewe, R. S.; Ewbank, P. C.; Liu, J. S.; Zhai, L.; McCullough, R. D. *Macromolecules* **2001**, *34*, 4324–4333.
(31) Iovu, M. C.; Sheina, E. E.; Gil, R. R.; McCullough, R. D. *Macromolecules* **2005**, *38*, 8649–8656.
(32) Yokoyama, A.; Miyakoshi, R.; Yokozawa, T. *Macromolecules* **2004**, *37*, 1169–1171.
(33) Ohshimizu, K.; Ueda, M. *Macromolecules* **2008**, *41*, 5289–5294.
(34) Ouhib, F.; Hiorns, R. C.; de Bettignies, R.; Bailly, S.; Desbrieres, J.; Dagron-Lartigau, C. *Thin Solid Films* **2008**, *516*, 7199–7204.
(35) Trznadel, M.; Pron, A.; Zagorska, M. *Macromolecules* **1998**, *31*, 5051–5058.
(36) Brown, P. J.; Thomas, D. S.; Kohler, A.; Wilson, J. S.; Kim, J. S.; Ramsdale, C. M.; Sirringhaus, H.; Friend, R. H. *Phys. Rev. B* **2003**, *67*, 420301–420316.
(37) Merlo, J. A.; Frisbie, C. D. *J. Phys. Chem. B* **2004**, *108*, 19169–19179.
(38) Berson, S.; De Bettignies, R.; Bailly, S.; Guillerez, S. *Adv. Funct. Mater.* **2007**, *17*, 1377–1384.
(39) Chen, T. A.; Wu, X. M.; Rieke, R. D. *J. Am. Chem. Soc.* **1995**, *117*, 233–244.
(40) Ihn, K. J.; Moulton, J.; Smith, P. *J. Polym. Sci., Part B: Polym. Phys.* **1993**, *31*, 735–742.
(41) Darling, S. B.; Sternberg, M. *J. Phys. Chem. B* **2009**, *113*, 6215–6218.
(42) van Eijck, L.; Johnson, M. R.; Kearley, G. J. *J. Phys. Chem. A* **2003**, *107*, 8980–8984.
(43) Wu, P. T.; Ren, G. Q.; Li, C. X.; Mezzenga, R.; Jenekhe, S. A. *Macromolecules* **2009**, *42*, 2317–2320.
(44) Frisch, M. J., Trucks, G. W.; Schlegel, H. B.; Scuseria, G. E.; Robb, M. A.; Cheeseman, J. R.; Montgomery, J. A., Jr.; Vreven, T.; Kudin, K. N.; Burant, J. C.; Millam, J. M.; Iyengar, S. S.; Tomasi, J.; Barone, V.; Mennucci, B.; Cossi, M.; Scalmani, G.; Rega, N.; Petersson, G. A.; Nakatsuji, H.; Hada, M.; Ehara, M.; Toyota, K.; Fukuda, R.; Hasegawa, J.; Ishida, M.; Nakajima, T.; Honda, Y.; Kitao, O.; Nakai, H.; Klene, M.; Li, X.; Knox, J. E.; Hratchian, H. P.; Cross, J. B.; Bakken, V.; Adamo, C.; Jaramillo, J.; Gomperts, R.; Stratmann, R. E.; Yazyev, O.; Austin, A. J.; Cammi, R.; Pomelli, C.; Ochterski, J. W.; Ayala, P. Y.; Morokuma, K.; Voth, G. A.; Salvador, P.; Dannenberg, J. J.; Zakrzewski, V. G.; Dapprich, S.; Daniels, A. D.; Strain, M. C.; Farkas, O.; Malick, D. K.; Rabuck, A. D.; Raghavachari, K.; Foresman, J. B.; Ortiz, J. V.; Cui, Q.; Baboul, A. G.; Clifford, S.; Cioslowski, J.; Stefanov, B. B.; Liu, G.; Liashenko, A.; Piskorz, P.; Komaromi, I.; Martin, R. L.; Fox, D. J.; Keith, T.; Al-Laham, M. A.; Peng, C. Y.; Nanayakkara, A.; Challacombe, M.; Gill, P. M. W.; Johnson, B.; Chen, W.; Wong, M. W.; Gonzalez, C.; Pople, J. A. *Gaussian 03W*; Gaussian, Inc.: Wallingford, CT, 2004.